J Eng Math (2009) 64:319–330
DOI 10.1007/s10665-009-9281-3

A 3D/1D geometrical multiscale model of cerebral vasculature

Tiziano Passerini · Mariarita de Luca · Luca Formaggia · Alfio Quarteroni · Alessandro Veneziani

Received: 26 May 2008 / Accepted: 23 February 2009 / Published online: 18 March 2009

Abstract Geometrical multiscale modeling is a strategy advocated in computational hemodynamics for representing in a single numerical model dynamics that involve different space scales. This approach is particularly useful to describe complex networks such as the circle of Willis in the cerebral vasculature. A multiscale model of the cerebral circulation is presented where a one-dimensional (1D) description of the circle of Willis, relying on the one-dimensional Euler equations, is coupled to a fully three-dimensional model of a carotid artery, based on the solution of the incompressible Navier–Stokes equations. Even if vascular compliance is often not relevant to the meaningfulness of three-dimensional (3D) results by themselves, it is crucial in the multiscale model, since it is the driving mechanism of pressure-wave propagation. Unfortunately, 3D simulations in compliant domains still demand computational costs significantly higher than in the rigid case. Appropriate matching conditions between the two models have been devised to concentrate the effects of the compliance at the interfaces and to obtain reliable results still solving a 3D problem on rigid vessels.

Keywords Circle of Willis · Domain splitting · Geometrical multiscale modeling · Matching conditions

1 Introduction

The complexity of the vascular system necessitates the set-up of convenient mathematical and numerical models surpassing the usual models in fluid dynamics. Basically, computational hemodynamics relies on three classes of models, featuring a different level of detail in the space dependence.

T. Passerini · M. de Luca · L. Formaggia · A. Quarteroni
MOX, Department of Mathematics, Politecnico di Milano, Milano, Italy

M. de Luca
Department of Mechanical Engineering, University of Pittsburgh, Pittsburgh, PA, USA

A. Quarteroni
CMCS, EPFL, Lausanne, Switzerland

A. Veneziani (✉)
Department of Mathematics and Computer Science, Emory University, Atlanta, GA, USA
e-mail: ale@mathcs.emory.edu

Fully three-dimensional (3D) models are based on the incompressible Navier–Stokes equations possibly coupled to appropriate models that describe the blood viscosity and the mechanical deformation of the vascular tissue. These models are well suited for investigating the effects of the geometry on the blood flow and the possible physio–pathological impact of hemodynamics. Unfortunately, the high computational costs restrict their use to contiguous vascular districts only on a space scale of a few centimeters or fraction of a meter at the most (see, e.g., [1]).

By exploiting the cylindrical geometry of vessels, it is possible to resort to *one-dimensional models* (1D), by reducing the space dependence to the vessel's axial coordinate only. These models are basically given by the well-known Euler equations and provide an optimal tool for the analysis of wave-propagation phenomena in the vascular system. They are convenient when the interest is in obtaining the pressure dynamics in a large part of the vascular tree at a reasonable computational cost (see [3,4] and [5, Chap. 10]). However, the space dependence still retained in these models inhibits their use for the whole vascular system. In fact, it would be unfeasible to follow the geometrical details of the whole capillary network.

A compartmental representation of the vascular system leads to a further simplification in the mathematical modeling, based on the *analogy between hydraulic networks and electrical circuits*. The fundamental ingredients of these *lumped-parameter (0D) models* are the Kirchhoff laws, which lead to systems of differential–algebraic equations. These models can provide a representation of a large part or even the whole circulatory system, since they get rid of the explicit space dependence. They can include the presence of the heart, the venous system, and self-regulating and metabolic dynamics in a simple way and at a low computational cost [3].

All these models have peculiar mathematical characteristics. They are able to capture different aspects of circulatory systems that, however, are coupled together in reality. In fact, the intrinsic robustness of the vascular system, still able to provide blood to districts affected by a vascular occlusion, thanks to the development of compensatory dynamics, strongly relies upon this coupling of different space scales. Feedback mechanisms essential to the correct functioning of the vascular system work over the space scale of the entire network, even if they are activated by local phenomena such as an occlusion or the local demand of more oxygen by an organ. This is particularly evident in one of the most important parts of the vascular tree, the cerebral vasculature. Circulation in the head features a strongly coupled anastomotic system, called the *circle of Willis*, which ensures an adequate blood supply to the brain, even when one of the incoming arteries is occluded or missing (see, e.g., [6–8]).

To devise numerical models able to cope with coupled dynamics ranging on different space scales, a *geometrical multiscale approach* has been proposed in [4], see Fig. 1. According to this approach, the three different classes of models are mathematically coupled in a unique numerical model. Despite the intuitiveness of this approach, many difficulties arise when trying to combine numerically mathematical models that are self-consistent but not

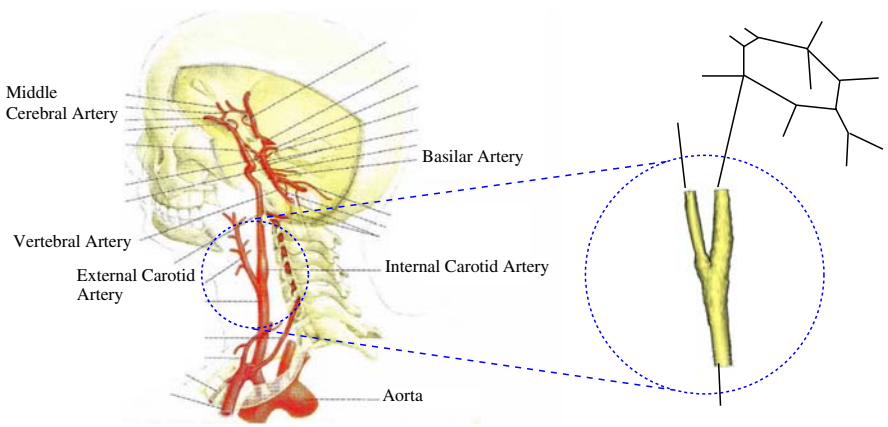

Fig. 1 *Left*: Anatomical representation of the cerebral vasculature, including the circle of Willis (after Balboni [2]). *Right*: Multiscale representation of the cerebral vasculature: a 3D representation of one of the carotid arteries is embedded in a 1D network of Euler problems

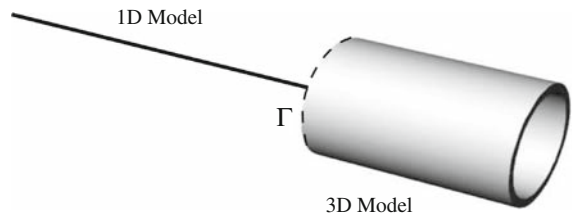

Fig. 2 A simple multiscale (3D/1D) model of a cylindrical pipe

designed to work together; see, e.g., [8,9]. Some of these difficulties have been extensively discussed recently in [5, Chap. 11].

A practical difficulty arises when some features that could be neglected at a certain scale become essential in the coupled model, inducing a significant increase of the overall computational cost. This is the case of the compliance of vessels. In 3D Navier–Stokes stand-alone models compliance is quite often not relevant for bioengineering purposes. However, it is a driving mechanism of pressure-wave propagation along the vascular tree. Therefore, when considering 3D/1D geometrical multiscale models, in principle compliance should not be disregarded in either models. The computational cost of a compliant 3D simulation is, however, by far (in general, more than two times) higher than for the rigid case. The coupling between 1D and 3D compliant models has been investigated recently in [10].

A naive coupling of the intrinsically compliant 1D model with a 3D rigid one, forcing for instance the continuity of pressure and flow rate at the interface, is problematic. The main reason is that the different mathematical modeling of the wall in the two subdomains causes spurious wave reflections at the interface between the models, strongly affecting the numerical results. We overcome these difficulties by resorting to appropriate matching conditions that mimic the presence of the compliance, by concentrating it at the interface between the models. We introduce these conditions in Sect. 2. In Sect. 3 we present a multiscale model of the circle of Willis based on a 1D network whose results are in good agreement with results taken from the literature (Sect. 3.1). We illustrate multiscale simulations where a 3D model of the left carotid bifurcation is coupled with the 1D model of the circle of Willis. Thanks to the adoption of matching conditions including the compliance, it is possible to simulate the overall dynamics still solving a 3D rigid model.

The fine-tuning of the parameters associated with the proposed interface conditions is briefly addressed in the Conclusions.

2 Matching conditions in 3D rigid/1D multiscale models

To fix the ideas, let us refer to the simple model represented in Fig. 2. We assume that a cylindrical pipe has been split at section Γ into two halves. The left one is described in terms of the 1D Euler equations

$$\frac{\partial A}{\partial t} + \frac{\partial Q}{\partial x} = 0, \quad \frac{\partial Q}{\partial t} + \frac{\partial}{\partial x}\left(\alpha \frac{Q^2}{A}\right) + \frac{A}{\rho}\left(\frac{\partial P}{\partial x}\right) + K_R \frac{Q}{A} = 0. \tag{1}$$

Here $A = A(t, x)$ represents the area of the vascular section at the abscissa x along the vessel axis and at time t; $Q = Q(t, x)$ is the corresponding flow rate, $P = P(t, x)$ is the pressure, ρ the blood density, assumed to be constant, α the so-called *momentum correction coefficient* and, under the assumption of a parabolic velocity profile, $K_R = 8\pi\mu$ is a coefficient associated with the blood viscosity μ; see, e.g., [3] and [5, Chap. 10] for more details. Following classical arguments for 1D models, we assume that the pressure and the radius of the vessel feature a linear dependence, or equivalently

$$P = \Psi(A) = P_{\text{ext}} + \frac{\sqrt{\pi} h_0 E}{(1 - \nu^2) A_0}\left(\sqrt{A} - \sqrt{A_0}\right), \tag{2}$$

where E is the Young modulus of the wall, h_0 is the wall thickness and ν the Poisson ratio. The flow in the right-hand side of the pipe is described by the incompressible Navier–Stokes equations

$$\rho\frac{\partial \mathbf{u}}{\partial t} + \rho\mathbf{u}\cdot\nabla\mathbf{u} - \nabla\cdot(\mu\nabla\mathbf{u}) + \nabla p = \mathbf{0}, \quad \nabla\cdot\mathbf{u} = 0, \tag{3}$$

where $\mathbf{u} = \mathbf{u}(x, y, z, t)$ is the velocity field, $p = p(x, y, z, t)$ the pressure.

Coupling the two models requires appropriate matching conditions. In the case of a rigid 3D model, it is reasonable to prescribe the continuity of pressure and flow rate

$$P_{1D} = \frac{1}{|\Gamma|}\int_\Gamma p_{3D}\mathrm{d}\gamma, \quad Q_{1D} = -\rho\int_\Gamma \mathbf{u}_{3D}\cdot\mathbf{n}\mathrm{d}\gamma, \tag{4}$$

where we have added the indexes $1D$ and $3D$ for the sake of clarity and denoted by $|\Gamma|$ the area of the interface Γ. The negative sign in the second equation of (4) stems from the fact that Q_{1D} and $\mathbf{u}_{3D}\cdot\mathbf{n}$ are pointing outwards from the 1D and 3D domains, respectively. In the sequel, for ease of notation, we set $Q_{3D} = \rho\int_\Gamma \mathbf{u}_{3D}\cdot\mathbf{n}\mathrm{d}\gamma$ and $P_{3D} = 1/|\Gamma|\int_\Gamma p_{3D}\mathrm{d}\gamma$.

Other conditions can be considered as well, e.g. prescribing the continuity of the total pressure, of the normal stresses or of the characteristic variables; see [5, Chap. 11].

When solving multiscale problems numerically, it is natural to split the scheme into an iterative sequence of dimensionally homogeneous problems, which we indicate as 1D and 3D, for instance by means of the following algorithm. We assume that standard (Dirichlet or Neumann) conditions are prescribed at the boundaries of the overall 1D/3D model. Moreover, we carry out an appropriate space and time discretisation of the problems. In particular, superscripts n and $n+1$ refer to the approximation of the solution at time steps t^n and t^{n+1}, respectively. Index k will refer to the inner iterations performed at a fixed time step, for the fulfillment of the matching conditions. For $n = 0, 1, \ldots$ we perform the following steps.

(1) `Initialization.` Set $k = 0$, $\mathbf{u}^{n+1}_{3D,0} = \mathbf{u}^n_{3D}$, $p^{n+1}_{3D,0} = p^n_{3D}$ and $P^{n+1}_{1D,0} = P^n_{1D}$, $A_{1D,0} = \psi^{-1}(P^{n+1}_{1D,0})$, $Q^{n+1}_{1D,0} = Q^n_{1D}$.

(2) `Loop` on k

(2.1) *Solve* the 1D model with the boundary condition on Γ given by

$$P^{n+1}_{1D,k+1} = \chi P^{n+1}_{3D,k} + (1-\chi)P^{n+1}_{1D,k}, \tag{5}$$

where χ is a relaxation parameter to be set for improving the convergence rate. Solving the 1D model, pressure conditions are recast in terms of area, thanks to the wall law $A^{n+1}_{1D,k+1} = \psi^{-1}(P^{n+1}_{1D,k+1})$.

(2.2) *Solve* the 3D problem with the boundary conditions on Γ

$$Q_{3D,k+1} = -Q^{n+1}_{1D,k+1} \tag{6}$$

Set $k = k + 1$.

(3) `Test.` Different convergence tests can be pursued. A possibility is to check the continuity at the interface, namely terminate the iterations when $|P^{n+1}_{1D,k+1} - P^{n+1}_{3D,k+1}| \le \varepsilon$ being ε a user-defined tolerance. Another possibility is to check the increments of the interface variables in subsequents iterations.

Swapping the role of the matching conditions in the set-up of the boundary conditions for the iterative scheme, (5), (6) can be replaced by

$$Q^{n+1}_{1D,k+1} = -\chi Q^{n+1}_{3D,k} + (1-\chi)Q^{n+1}_{1D,k}, \quad P^{n+1}_{3D,k+1} = P^{n+1}_{1D,k+1}. \tag{7}$$

The different space dependence of 1D and 3D models leads to unmatched or defective conditions (step 2 of the loop) and in particular (6) (or the second condition (7)) do not prescribe sufficient conditions for the closure of the Navier–Stokes problem. The latter needs to be solved in the framework of *defective boundary problems*, the data available at the boundary being insufficient to guarantee the uniqueness of the solution. This topic has been discussed in [5, Chap. 11], where different mathematically sound techniques for the solution of defective problems

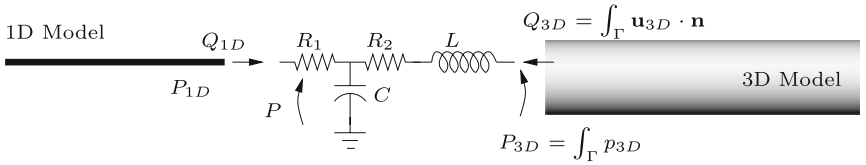

Fig. 3 Representation of a multiscale model with a 0D element representing the compliance of the 3D model at the interface

are presented. The specific method for solving the 3D problem affects the accuracy of the Navier–Stokes solution and is not relevant for the purpose of the present paper, so we do not dwell upon it. Any reasonable technique can be used in the context of our multiscale modeling.

The iterative approach given by the previous three steps suffers from numerical problems induced by the different description of the wall mechanics in the two halves of the pipe, which produces spurious reflections at the interface and possible numerical instabilities. One could avoid this kind of problems by resorting to a compliant 3D model. As we have pointed out, this increases the computational costs strongly. More precisely, implicit coupled fluid–structure iterative schemes at each time step require to solve the Navier–Stokes and the structural problems several times. In explicit coupled fluid–structure iterative schemes, stability concerns typically require to take small time steps.

In the next subsection, we present a different strategy based on the set-up of an appropriate set of interface conditions.

2.1 Matching conditions including compliance

2.1.1 A simple case

Suppose we have a simplified representation of the compliance of the 3D vessel in the multiscale model by gathering its effect at the interface using a special lumped-parameter model. Referring for instance to Fig. 3, we introduce a *RCL network* at the interface with the role of representing the effects of the compliance of the artery in the 3D model. In this way, we still use a 3D rigid model which, however, behaves like a compliant one with respect to the system dynamics. By denoting with P the pressure associated with the capacitance C, we can derive the following set of equations (see, e.g., [5, Chap. 10] and [11]):

$$P = P_{1D} - R_1 Q_{1D}, \quad P = P_{3D} - L\frac{\mathrm{d}Q_{3D}}{\mathrm{d}t} - R_2 Q_{3D}, \quad C\frac{\mathrm{d}P}{\mathrm{d}t} = Q_{1D} + Q_{3D}. \tag{8}$$

Taking the derivative of the first equation and using the third, we can eliminate P and finally obtain the new conditions in the iterative scheme, by replacing (5) and (6) with

$$\begin{aligned} P_{1D,k+1} = \chi \Bigg(& P_{3D,k} - L_1\frac{\mathrm{d}Q_{3D,k}}{\mathrm{d}t} - R_2 Q_{3D,k} + R_1 C_1 \frac{\mathrm{d}P_{3D,k}}{\mathrm{d}t} \\ & - R_1 C L \frac{\mathrm{d}^2 Q_{3D,k}}{\mathrm{d}t^2} - R_1 C R_2 \frac{\mathrm{d}Q_{3D,k}}{\mathrm{d}t} - R_1 Q_{3D,k} \Bigg) + (1-\chi) P_{1D,k} \\ Q_{3D,k+1} = & -Q_{1D,k+1} + C\frac{\mathrm{d}P_{1D,k+1}}{\mathrm{d}t} - R_1 C \frac{\mathrm{d}Q_{1D,k+1}}{\mathrm{d}t}. \end{aligned} \tag{9}$$

These conditions (hereafter denoted by *LP* (Lumped Parameter) *conditions*) involve time derivatives of the matching quantities. They have been discretized with finite differences of the same accuracy of the time-advancing scheme used for the time discretisation of the Navier–Stokes and Euler equations. More precisely, in this work we resorted to the first-order implicit finite differences.

Remark As expected, for $C = 0$, $R_1 = R_2 = 0$ and $L = 0$ we recover the coupling given by conditions (5), (6). This corresponds physically to the case of a rigid portion of artery in a network of compliant vessels, as it is the case of a stented or prosthetic segment; see [12].

2.1.2 Parameters estimation

The interface LP model of Fig. 3 provides a physical representation of our matching conditions. A major issue in this approach is the tuning of the paramaters featuring the LP model. In particular, we started from a classical RCL network, advocated for representing the capillary circulation; see [13–15].

We remind that, following classical arguments for the derivation of lumped-parameter models (see, e.g., [5, Chap. 10], based on a proper average of the Navier–Stokes equations) for a cylindrical vessel with length l, area A_0, with a linear elastic wall with thickness h_0 and Young modulus E, the compliance may be estimated to be $C \propto A_0^{3/2} l/(Eh_0)$. Physiological values of this parameter are of the order of $10^{-5}\,\mathrm{cm}^5/\mathrm{dyn}$. In our computation ($l = 5\,\mathrm{cm}$ and $A_0 = \pi\,\mathrm{cm}^2$) we set $C = 5.8910^{-5}\,\mathrm{cm}^5/\mathrm{dyn}$. The other parameters have been properly adjusted in order to reduce spurious effects at the 1D/3D interfaces. More precisely, resistance R_1 has been introduced in [15] and, following the proposal of that paper, it is dynamically selected so that an incoming wave from the 1D model is propagated without any reflection. For R_2 and L, in this paper we have adopted an empirical trial-and-error approach, so that after some numerical experiments we put $R_2 = 1\,\mathrm{dyn\,s\,cm}^{-2}$ and $L = 0.01\,\mathrm{g\,cm}^{-4}$.

For more complex models, these parameters should be adapted accordingly. A mathematically sound approach for the fine-tuning of the parameters is beyond the scope of the paper (see the Conclusion section). Here, we have adopted a trial-and-error approach.

The impact of the LP conditions is illustrated in Figs. 4 and 5. More precisely, in Fig. 4 we show results obtained for the model of Fig. 3 when a sinusoidal waveform for the flow rate is prescribed at the inlet. We compare the time history of the flow rate and area (as a function of the pressure) at the interface, denoted by Q_{1D} and $A(P_{1D})$ in Fig. 3, obtained with a standard multiscale 1D/3D model, using the proposed approach and finally those obtained with a complete 1D model. In Fig. 5 we present similar comparisons for the case when a step waveform is prescribed at the inlet of the domain. The impact of interface conditions is evident. In the case based on classical matching, the solution is dramatically affected by reflections induced by the different description of the wall mechanics in the 1D and 3D model. These reflections change completely the profile of the solution. Observe that the complete reflection of the flow rate of Fig. 5 can be justified by a linear analysis of the reflection coefficient considered e.g. in [2]. For a rigid downstream pipe, this coefficient corresponds to total reflection. On the contrary, matching conditions based on the RCL model are able to obtain a behavior similar to that of the complete 1D model, even if we are using a rigid 3D model. The same conclusions hold for the area: the RCL-based conditions allow us to find a solution significantly close to that of the complete 1D model. As pointed out, a proper tuning of the parameters is crucial to find the best RCL model.

2.2 A 1D–3D–1D coupling

Let us now consider the case represented in Fig. 6, where we show a sequence of 1D–3D–1D models with appropriate LP conditions. From a numerical point of view on the left interface we still resort to the iterative scheme with conditions (9). On the right interface, we adopt a similar iterative strategy where we prescribe a pressure condition to the 3D problem and flow rate conditions to the 1D Euler system downstream. More precisely, equations corresponding to the downstream interface read

$$\begin{cases} P_{3D} - R_3 Q_{3D} = P_{1D} - L_2 \dfrac{\mathrm{d}Q_{1D}}{\mathrm{d}t} - R_4 Q_{1D} \\ C_2 \dfrac{\mathrm{d}P_{3D}}{\mathrm{d}t} - R_3 C_2 \dfrac{\mathrm{d}Q_{3D}}{\mathrm{d}t} = Q_{1D} + Q_{3D} \end{cases}$$

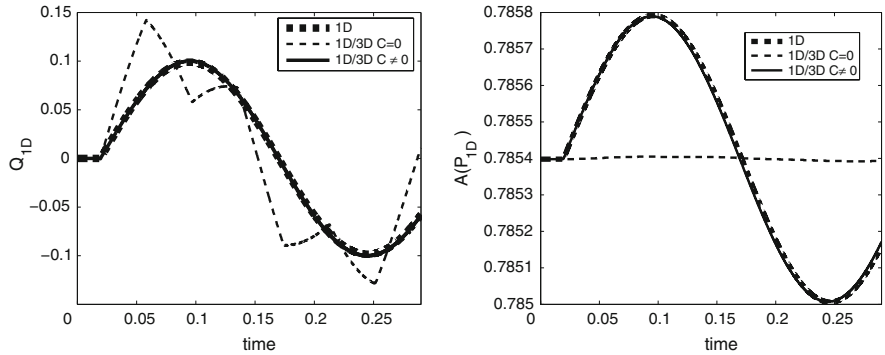

Fig. 4 Comparison of dynamics of flow rate (*left*) and area (*right*) at $x = 5$ cm of a compliant pipe simulated with a fully 1D model, a multiscale 1D/3D model with direct coupling and with the matching conditions obtained by the lumped-parameter models. The input waveform of the flow rate at the tube inlet is a sine with amplitude 0.1. (time in [s], volumetric flow rate in [cm^3/s], area in [cm^2])

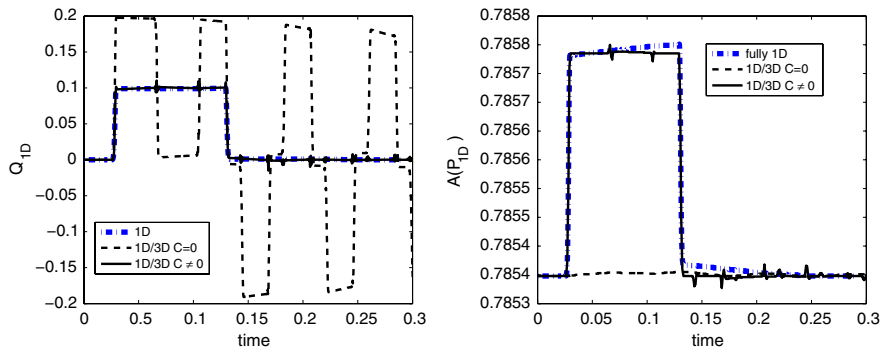

Fig. 5 Comparison of dynamics of flow rate (*left*) and area (*right*) at $x = 5$ cm of a compliant pipe simulated with a fully 1D model, a multiscale 1D/3D model with direct coupling and with the matching conditions obtained by the lumped-parameter models. The input waveform of the flow rate at the tube inlet is a step function with amplitude 0.1. (time in [s], volumetric flow rate in [cm^3/s], area in [cm^2])

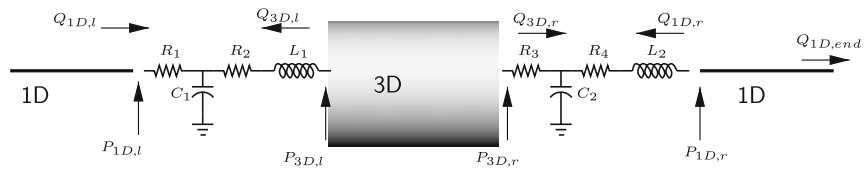

Fig. 6 Representation of a multiscale model with two-buffer 0D elements at the interface

Consequently, the coupling conditions used in the iterative scheme are

$$\begin{cases} Q_{1D,k+1} = \chi\left(-Q_{3D,k} + C_2\dfrac{\mathrm{d}P_{3D,k}}{\mathrm{d}t} - R_3C_2\dfrac{\mathrm{d}Q_{3D,k}}{\mathrm{d}t}\right) + (1-\chi)Q_{1D,k} \\ P_{3D,k+1} = P_{1D,k+1} - L_2\dfrac{\mathrm{d}Q_{1D,k+1}}{\mathrm{d}t} - R_4Q_{1D,k+1} + R_3C_2\dfrac{\mathrm{d}P_{1D,k+1}}{\mathrm{d}t} \\ \qquad\qquad -R_3C_2L_2\dfrac{\mathrm{d}^2Q_{1D,k+1}}{\mathrm{d}t^2} - R_3C_2R_4\dfrac{\mathrm{d}Q_{1D,k+1}}{\mathrm{d}t} - R_3Q_{1D,k+1} \end{cases} \tag{10}$$

Numerical results are reported in Fig. 7. Again, we illustrate the comparison of the solutions obtained with a 1D model, and the multiscale models corresponding to Fig. 6, where all the lumped parameters are null (classical conditions) and when they are activated. The inlet waveform is sinusoidal.

In the first picture we present the flow rate at the first interface (denominated $Q_{1D,l}$ in Fig. 6), in the second the flow rate $-Q_{1D,r}$ at the second interface and finally the flow rate $Q_{1D,\mathrm{end}}$ at the outlet of the right pipe. Again, when

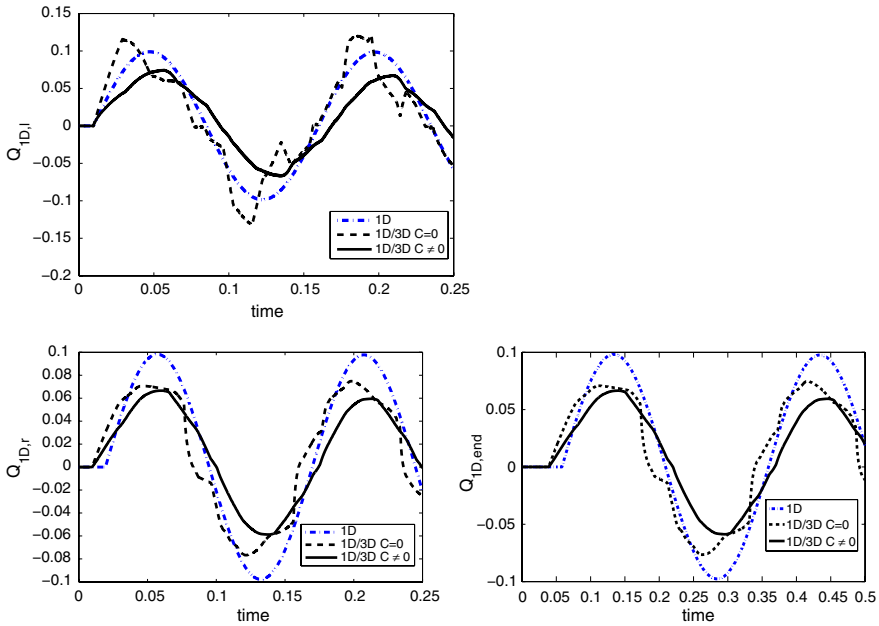

Fig. 7 Comparison of flow rates computed by a 1D model (*dash-dot line*), a multiscale 1D/3D/1D model with classical matching conditions (*dashed line*) and with lumped-parameter matching conditions (*solid line*) in correspondence of the first interface (*top*), the second (*bottom, left*) and the outlet of the domain (*bottom, right*). (time in [s], volumetric flow rate in [cm^3/s])

classical matching conditions are used (corresponding to null values of the parameters) the superposition of the wave components induced by reflections triggered by the different wall models at the inlet is evident. This changes the shape of the propagating wave and affects both the amplitude and the phase at the inlet and at the outlet of the 3D model. Amplitude dissipation in the forward component of the wave is partially compensated by the superimposition of the spurious reflections. In the case of LP conditions, the shape of the wave is only partially affected. Dispersion errors are remarkably small, whilst dissipation effects are present. More precisely, the dispersion error, evaluated as the difference in the occurrence of the peaks in the 1D and the multiscale LP models, are 20%, 6% and 5% in the three pictures of Fig. 7, respectively, while dissipation, evaluated as the difference of the peaks, are 25%, 32% and 32%, respectively. The impact of finite-difference schemes in the numerical implementation of matching conditions is probably the main factor responsible for these effects. A more accurate analysis of this aspect will be carried out elsewhere. In any case matching conditions guarantee a significant reduction of spurious reflections.

3 Multiscale model of the circle of Willis

The circle of Willis is the main collateral pathway of the cerebral circulation. It is essentially given by a polygonal ring at the basis of the brain . The polygon (see Fig. 8) is made of the right and left Posterior Cerebral Arteries (rPCA and lPCA), the right and left Posterior Communicating Arteries (rPCoA and lPCoA), the right and left Anterior Cerebral Arteries (rACA and lACA) and the Anterior Communicating Artery (ACoA). Blood is supplied by the two Internal Carotid Arteries (rICA and lICA) and the two Vertebral Arteries (rVA and lVA). The latter join into the Basilar Artery (BA), from which the two PCAs depart, delivering blood in the posterior region of the brain. The two ACAs depart from the ICAs and deliver blood to the anterior part of the brain. This complex structure has two advantages. On the one hand, it supplies blood to the brain, even when one or more vessels are occluded or missing. On the other hand, it protects the brain from excessive supply of blood, distributing it uniformly.

It is well known that in fact in almost 50% of the population one of the branches of the circle is absent or partially developed [16]. A correct knowledge of the functioning of the circle of Willis is relevant in clinical practice for many

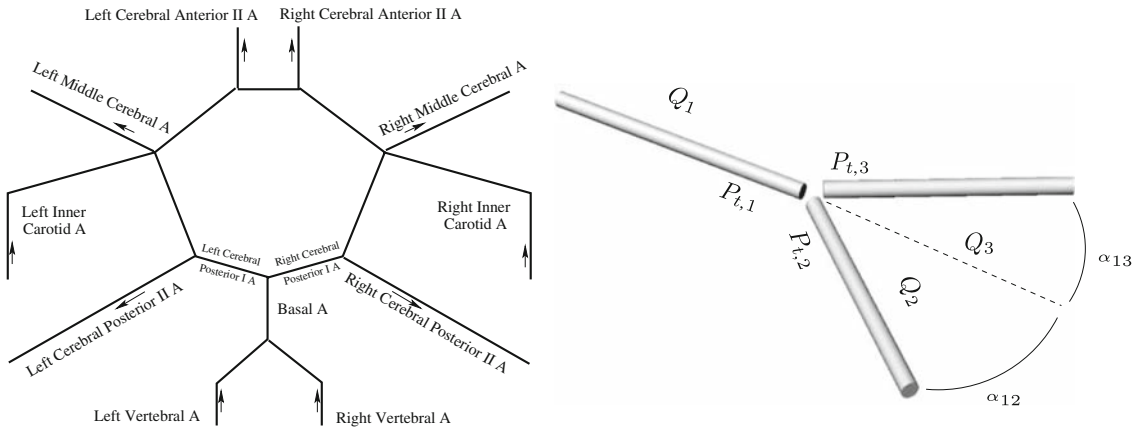

Fig. 8 1D model of the circle of Willis: description of the circle (*left*) and a bifurcation (*right*)

intracranial or extracranial procedures like endoarterectomy, carotid stenting or the compression carotid test; see, e.g., [17]. Several mathematical studies have been carried out for devising quantitative analysis of this district. After the first studies based on hydraulic or electric analog models [18–21], we mention the investigations carried out in [22]. Most of the research is based on modeling the circle of Willis as a set of 1D Euler problems (1) representing each branch of the circle, with an appropriate modeling of the bifurcations. We further mention [6,15,23–27]. More recently, metabolic models have been added to simulate cerebral auto-regulation, which is a feedback mechanism driving an appropriate blood supply into the circle on the basis of oxygen demand by the brain [15]. A complete 3D image based numerical model of the circle of Willis has been presented in [1]. It requires medical data that are currently beyond the usual availability in common practice, and is computationally intensive. Hereafter, we propose a multiscale model where the 3D simulation is used only in the region of interest (the left ICA in our case) and the remainder of the network is modeled by a 1D network. A similar multiscale model has been investigated in [10], where the 3D model includes compliance for avoiding spurious reflections induced by a rigid treatment of the 3D geometry in the multiscale model. Here we discuss results obtained with a rigid model together with the lumped-compliance matching conditions just described.

3.1 The 1D network

The proposed model is based on the set-up presented by Alastruey et al. [15] for the description of the cerebral circulation. The circle of Willis is immersed in a larger network of 1D models describing the main arteries bringing blood to the brain, and the inflow boundary condition for the whole network is provided by the heart.

In our model, the vascular network is represented by an oriented graph. The edges of the graph correspond to the vessels, while the nodes are the junctions. Each edge (see Fig. 8 on the left) has been described by system (1) where appropriate initial conditions have been assumed. The junctions have been modeled by prescribing balance equations for the mass and the total pressure $P_t = P + 1/2\rho U^2$ (see [12,28]). For the sake of concreteness, if we refer to Fig. 8 on the right, we will prescribe

$$Q_1 + Q_2 + Q_3 = 0, \quad \begin{array}{l} P_{1,t} = P_{2,t} + \varphi(U, \alpha_{12}) \\ P_{1,t} = P_{3,t} + \varphi(U, \alpha_{13}) \end{array},$$

where functions φ possibly include some dissipation effects depending on the bifurcation angles α_{12} and α_{13}. We assume $\varphi = 0$, since the numerical solution has been proved to be weakly affected by this choice; see [12].

The inlet condition is a periodic function of time representing the cardiac input, with period $T = 1\,\mathrm{s}$ [15]:

$$Q(t) = \begin{cases} 485 \cdot \sin\left(\frac{2\pi}{T} t\right) & 0 \le t < \tau_s \\ 0 & \tau_s \le t < T \end{cases}$$

with $\tau_s = 0.3\,\mathrm{s}$.

Table 1 Flow distribution in Anterior Cerebral Arteries (ACA), Middle Cerebral Arteries (MCA) and Posterior Cerebral Arteries (PCA) computed in different models proposed in the literature and in the present one

Model	ACA (%)	MCA (%)	PCA (%)
Hillen [23]	22.2	45.0	32.8
Hillen [24]	22.1	44.8	33.1
Lyden [25]	21.2	53.6	25.2
Macchi [26]	23.2	53.4	42.4
Viedma [6]	24.5	49.9	27.8
Ferrandez [27]	22.3	49.9	34.9
Our model	20.8	44.9	34.3

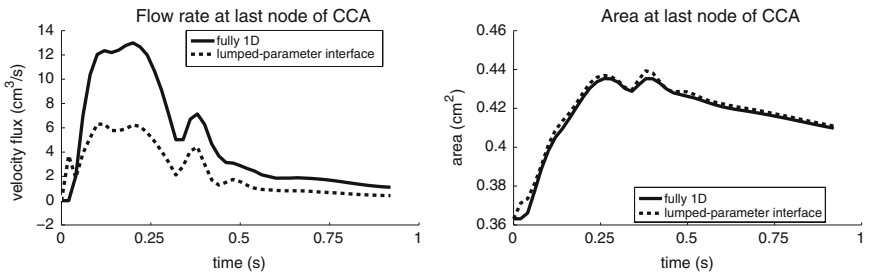

Fig. 9 Comparison of the results obtained with a fully 1D model (*solid line*) and the 3D rigid with RCL conditions at the inlet of Common Carotid Artery (*dashed line*). *Left*: flow rate, *Right*: area. (time in [s], volumetric flow rate in [cm^3/s], area in [cm^2])

At the outlet of the network we prescribe boundary conditions suitable for the representation of the capillary network. More precisely, we adopt a three-elements Windkessel model for the peripheral circulation as proposed in [14,15].

To check the reliability of our code we have reported in Table 1 the distribution of fluxes obtained by models of the circle of Willis available in the literature and our results. The agreement is good.

3.2 The 3D carotid model and the multiscale coupling

The multiscale model is depicted in Fig. 1, on the right. The geometry of the Left Internal Carotid geometry is based on the realistic model by Liepsch; see [29]. The Navier–Stokes equations in the 3D model have been solved with the code LifeV—see www.lifev.org—based on a $P1P1$ finite-element solver stabilized by means of an interior penalty approach. At the interfaces between the 3D and 1D models we prescribe conditions (9) at the upstream interface and conditions (10) at the downstream interfaces.

In Figs. 9 and 10, we present the results, in comparison with the ones of a fully 1D model. Results underline that the RCL-based conditions can actually obtain good solutions, in particular at the inlet. At the outlets of the carotid arteries the solution is strongly dissipated in the flow rate, while dispersion error and the area solution are in remarkably good agreement. Impact of the time discretisation of the matching conditions and the selection of the parameters on the dissipation error is under investigation.

4 Conclusions

We have proposed to introduce special matching conditions in a geometrical multiscale model of the circulatory system. In particular, we have considered the coupling of 1D and 3D models. The former intrinsically account for

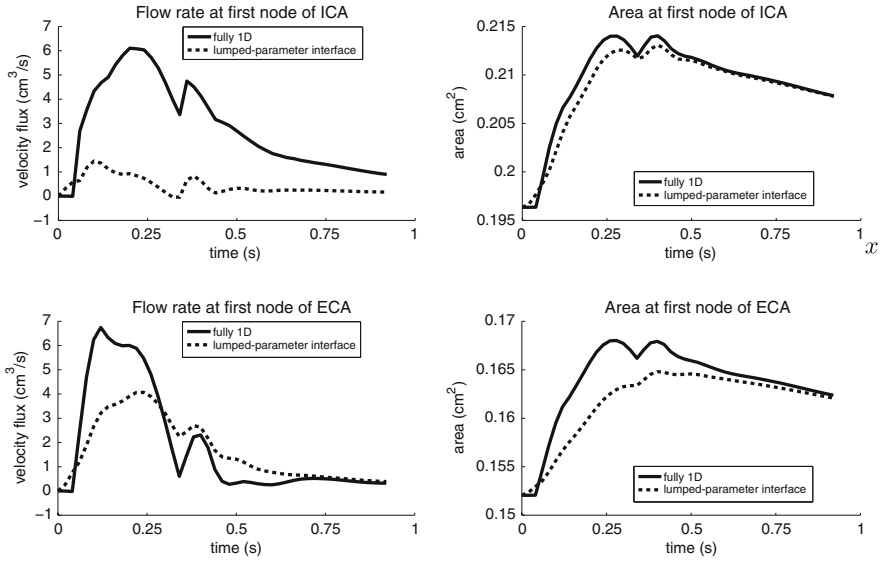

Fig. 10 Comparison of the results obtained with the fully 1D model (*solid line*) and the 3D rigid with RCL conditions in the branches (*dashed line*). *Top*: *Left*: flow rate in the Internal Carotid Artery (ICA), *Right*: area in the ICA. *Bottom*: *Left*: flow rate in the External Carotid Artery (ECA), *Right*: area in the ECA. (time in [s], volumetric flow rate in [cm^3/s], area in [cm^2])

vessel compliance, while the inclusion of wall mechanics in the latter induces a remarkable increment of the computational costs. On the other hand, even if the local effects of wall dynamics in the 3D stand-alone model are not significant, deformability is the driving mechanism of pressure-wave propagation dynamics over the arterial tree, so that it cannot be neglected in the multiscale framework. Matching conditions proposed here can be represented as a lumped-parameter model gathering the compliance at the interfaces between 1D (compliant) and 3D (rigid) models. In this way, deformability is included in the entire multiscale model, without resorting to expensive solutions of 3D fluid–structure interaction models.

For simple multiscale models, where the parameter quantification for the matching conditions is straightforwardly suggested by the mathematical derivation of the model, numerical results are really promising, showing that the multiscale 3D/0D/1D model can both capture the correct wave propagation (in comparison with a fully 1D model) and compute the local 3D flow. In more complex situations, like the circle of Willis in the cerebral vasculature, when a direct physiological quantification of the parameters is missing, results are only partially good. More precisely, at the inlet of the 3D model results still compare correctly with a fully 1D model, while downstream with respect to the 3D model dissipation effects in the flow rate are dominant.

A mathematically sound fine-tuning of the parameter is required. This goal can be pursued by a systematic sensitivity analysis or by extensive comparisons with stand-alone fully 3D models; see, e.g., [14,30]. This subject will be investigated in forthcoming papers together with a validation of this approach in more complex networks.

We finally point out that this approach can be extended to hydraulic networks featuring compliant pipes, beyond the specific medical applications considered here.

Acknowledgments A. Quarteroni, L. Formaggia and A. Veneziani are supported by the Project "Mathematical and numerical modelling of the electro-fluid-mechanics of the Heart" granted by the National Institute of High Mathematics (INDAM), Italy. T. Passerini, M. de Luca and A. Veneziani are supported by the Aneurisk Project, granted by Fondazione Politecnico di Milano and SIEMENS Medical Solutions, Italy.

References

1. Cebral JR, Castro MA, Soto O, Lohner R, Alperin N (2003) Blood-flow models of the circle of Willis from magnetic resonance data. J Eng Math 47:369–386

2. Balboni G. Anatomia Umana 1. Ediz. Ermes
3. Mynard JP, Nithiarasu P (2008) A 1D arterial blood flow model incorporating ventricular pressure, aortic valve and regional coronoary flow using the locally conservative Galerkin (LCG) method. Commun Numer Methods Eng 24:367–417
4. Formaggia L, Nobile F, Quarteroni A, Veneziani A (1999) Multiscale modelling of the circulatory system: a preliminary analysis. Comput Visual Sci 2(2/3):75–83
5. Quarteroni A, Formaggia L, Veneziani A (eds) (2009) Cardiovascular mathematics Springer. http://www.springer.com/math/applications/book/978-88-470-1151-9
6. Viedma A, Jimenez Ortiz C, Marco V (1997) Extended Willis circle model to explain clinical observations in periorbital arterial flow. J Biomech 30:265–272
7. Alastruey J, Moore SM, Parker KH, David T, Peirò J, Sherwin SJ (2008) Reduced modelling of blood flow in the cerebral circulation: coupling 1D, 0-D and cerebral autoregulation models. Int J Num Methods Fl 56:1061–1067
8. Ferrandez A, David T, Brown MD (2002) Numerical models of auto-regulation and blood flow in the cerebral circulation. Comput Methods Biomech Biomed Eng 5(1):7–19
9. Vignon I, Figueroa CA, Jansen KC, Taylor CA (2006) Outflow boundary conditions for three-dimensional finite element modeling of blood flow and pressure in arteries. Comput Methods Appl Mech Eng 195:3776–3796
10. Moura A (2007) The geometrical multiscale modelling of the cardiovascular system: coupling 3D FSI and 1D models, Mox PhD Thesis, Department of Mathematics, Politecnico di Milano, Italy
11. Quarteroni A, Veneziani A (2003) Analysis of a geometrical multiscale model based on the coupling of PDE's and ODE's for Blood Flow Simulations. Mult Models Sim SIAM 1(2):173–195
12. Formaggia L, Lamponi D, Quarteroni A (2003) One-dimensional models for blood flow in arteries. J Eng Math 47:251–276
13. Stergiopulos N, Westerhof BE, Westerhof N (1999) Total arterial inertance as the fourth element of the Windkessel model. Am J Physiol 276:H81–H88
14. Alastruey J, Parker KH, Peirò J, Sherwin SJ (2008) Lumped parameter outflow models for 1D blood flow simulations: effects on pulse waves and parameter estimation. Commun Comp Phys 4:317
15. Alastruey J, Parker KH, Peirò J, Byrd SM, Sherwin SJ (2007) Modelling the circle of Willis to assess the effects of anatomical variations and occlusions on cerebral flows. J Biomech 40:1794–1805
16. Lippert H, Pabst R (1985) Arterial variations in man: classification and frequency. JF Bergmann, Munich
17. Hetzel A, von Reuternc G-M, Wernza MG, Drostea DW, Schumacher M (2000) The carotid compression test for therapeutic occlusion of the internal carotid artery. Cerebrovasc Dis 10:194–199
18. Rogers L (1947) The function of the circulus arteriosus of Willis. Brain 70:171–178
19. Avman N, Bering EA (1961) A plastic model for the study of pressure changes in the circle of Willis and major cerebral arteries following arterial occlusion. J Neurosurg 18:361–365
20. Murray KD (1964) Dimensions of circle of Willis and dynamic studies using electrical analogy. J Neurosurg 21:26
21. Fasano VA, Broggi G (1966) Discussion sur le polygone de Willis. Neurochirurgie 12:761
22. Clark ME, Himwich WA, Martin JD (1967) Simulation studies of factors influencing cerebral circulation. Acta Neurol Scand 43:189
23. Hillen B (1986) On the meaning of the variability of the circle of Willis. Acta Morphol Neerlando-Scand 24:79–80
24. Hillen B, Drinkenburg BAH, Hoogstraten HW, Post L (1988) Analysis of flow and vascular resistance in a model of the circle of Willis. J Biomech 21:807–814
25. Lyden P, Nelson T (1997) Visualization of the cerebral circulation using three-dimensional transcranial power Doppler ultrasound imaging. J Neuroimag 7:35–39
26. Macchi C, Catini C, Federico C et al (1996) Magnetic resonance angiographic evaluation of circulus arteriosus cerebri (circle of Willis): a morphology study in 100 human healthy subjects. Ital J Anat Embryol 101:115–123
27. David T, Brown M, Ferrandez A (2003) Auto-regulation and blood flow in the cerebral circulation. Int J Numer Methods Fluids 43:701–713
28. Matthys KS, Alastruey J, Peirò J, Khir AW, Segers P, Verdonck PR, Parker KH, Sherwin SJ (2007) Pulse wave propagation in a model human arterial network: assessment of 1-D numerical simulations against in vitro measurements. J Biomech 40:3476–3486
29. Prosi M, Zunino P, Perktold K, Quarteroni A (2005) Mathematical and numerical models for transfer of low-density lipoproteins through the arterial walls: a new methodology for the model set up with applications to the study of disturbed lumenal flow. J Biomech 38(4):903–17
30. Martin V, Clement F, Decoene A, Gerbeau JF (2005) Parameter identification for a one-dimensional blood flow model. Proceedings Cemracs 2004, Esaim, September 2005